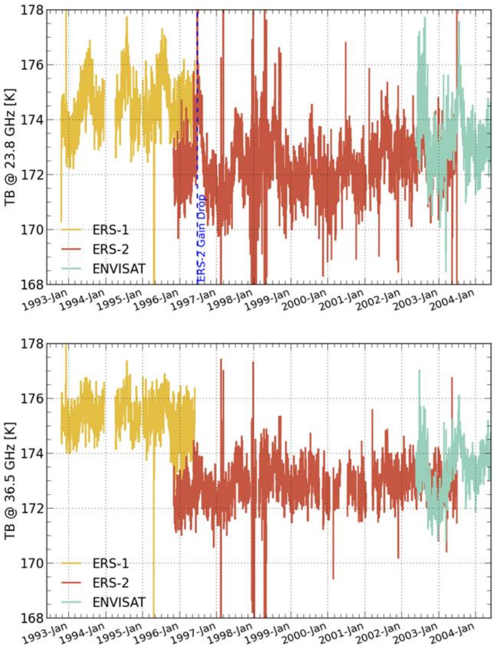

MWR Tb datasets (valid ocean) provided to the EMiR consortium. Top: 23.8 GHz channel for ERS-1 (gold), ERS-2 (red), and Envisat (turquoise). Bottom: As above, but for the 36.5 GHz channel.

ESA contract

4000109537/13/I-AM

ERS/Envisat MWR Recalibration and Water Vapour TDR Generation (EMiR)

MWR calibration assessment

(DLV-EXT-06)

Berlin, 6 October 2015

Document control sheet		
Project	ERS/Envisat MWR Recalibration and Water Vapour TDR Generation (EMiR)	
Client	European Space Agency, ESRIN Via Galileo Galilei, Casella Postale 64 00044 Frascati, Italy http://www.esa.int	
Main contractor	Informus GmbH Belziger Str. 44 10823 Berlin, Germany http://www.informus.de	
Title	MWR calibration assessment	
Status	Released	
Authors	Ralf Bennartz, Hannes Diedrich, Frank Fell, Bruno Picard, Martin Stengel, Oliver Sus	
Distribution	EMiR consortium, ESA	
Version control	2015-04-22	0.9, first draft
	2015-04-24	0.91, revised draft
	2015-05-06	1.0, initial version
	2015-07-14	1.1, revised version
	2015-10-06	1.2, FCDR and TCDR replaced by FDR and TDR
	2017-2-20	1.21, metadata harmonised

Table of contents

List of tables

List of figures

Executive summary

The calibration of satellite-based instruments is a critical first step toward the generation of Fundamental Data Records (FDR). This document describes a calibration assessment performed on ERS-1, ERS-2, and Envisat Microwave Radiometer (MWR) observations. The comparison was performed comparing a recently (December 2014) updated version of the REAPER MWR brightness temperature dataset to independent radiative transfer models. The comparison has revealed that the calibration of MWR is stable and that the instruments on board ERS-2 and Envisat appear to be well inter-calibrated.

Globally and annually averaged biases between ERS-2 and Envisat MWR observations and simulations are approximately +3 K for 23.8 GHz and +6 K for 36.5 GHz using RTTOV. Compared with other radiative transfer models also applied in this study, RTTOV shows the smallest bias values. MWR observations from ERS-1 are biased by an additional ca. +2 K in both channels as compared to ERS-2 and Envisat. This is in agreement with an independent assessment performed by CLS for the MWR on Envisat only.

Causes for the observed biases include the difficult absolute calibration of microwave instruments as well as uncertainties in the radiative transfer, surface emissivity, and spectroscopic models used. An investigation of the variability of these biases reveals a high degree of stability so that effective bias-correction and inter-calibration schemes can be devised in the next stage of the project.

1 Introduction

1.1 Purpose

This document provides an assessment of the calibration of the Microwave Radiometer (MWR) suite on board the satellites ERS-1, ERS-2 and Envisat. The data record analysed herein has been created specifically for the EMiR project from the official REAPER L1B dataset. Based on the results of the MWR calibration assessment, a number of recommendations are devised towards generating an improved MWR Fundamental Data Record (FDR) and derived L2 products.

1.2 Acronyms and abbreviations

Acronym	Description
AATSR	Advanced Along-Track Scanning Radiometer
ATBD	Algorithm Technical Basis Document
CLS	Collecte Localiation Satellites
DUE	Data User Element
ECMWF	European Centre for Medium-Range Weather Forecasts
EMiR	ERS/Envisat MWR Recalibration and Water Vapour FDR Generation
Envisat	Environmental Satellite
ERA-Interim	Global atmospheric reanalysis from 1979 to present by ECMWF
ERS	European Remote Sensing satellite
ESA	European Space Agency
ESL	Expert Support Laboratory
FAME-C	Freie Universität Berlin AATSR MERIS Cloud
FASTEM	Fast Microwave Emissivity Model
FDR	Fundamental data record
L1	Level 1 processing
L2	Level 2 processing
LWP	Liquid water path
MODIS	Moderate-resolution Imaging Spectroradiometer
MWR	Microwave Radiometer
OLCI	Ocean and Land Colour Instrument
OPR	Ocean product
PDS	Payload data
RA-2	Radar Altimeter (on board Envisat)
REAPER	Reprocessing of Altimeter Products for ERS
RTTOV	Radiative Transfer for TOVS
SLSTR	Sea and Land Surface Temperature Radiometer
SOI	Successive order of interaction
SST	Sea surface temperature
STDV	Standard deviation
SWH	Significant wave height
SWS	Surface wind speed

TB	Brightness temperature
TDR	Thematic data record
TCWV	Total column water vapour
WTC	Wet tropospheric correction

1.3 Reference documents

[RD-01] Picard, B. (2014): Presentation and recommendations on ERS-1/ERS-2 radiometer products, CLS-DOS-NT-14-203, issue 2, revision 0, 25/12/2014.

[RD-02] Eymard, L., and E. Obligis (2003): ERS2/MWR drift evaluation and correction, CLS-DOS-NT-03-688, issue 1, revision 0, 20/02/2003.

[RD-03] Stengel, M., R. Bennartz, F. Fell, and O. Sus (2015): MWR Level-2 Algorithm Theoretical Basis Document, Version 1.2, 06/05/2015.

[RD-04] Hollstein, A., Fischer, J., Carbajal Henken, C., and Preusker, R. (2015): Bayesian cloud detection for MERIS, AATSR, and their combination, *Atmos. Meas. Tech.*, 8, 1757-1771, DOI: http://dx.doi.org/10.5194/amt-8-1757-2015.

[RD-05] Bormann, N., A. Geer, and S. English (2012): Evaluation of the microwave ocean surface emissivity model FASTEM-5 in the IFS, Technical Memorandum No. 667, February 2012, 18 pages, ECMWF Research Department, Reading, UK.

[RD-06] RTTOV v6 Science and validation report, version 2 (2010): 30 pages. Available from https://nwpsaf.eu/deliverables/rtm/rtm_rttov6.html.

[RD-07] Heidinger, A. k., C. O'Dell, R. Bennartz, and T. Greenwald (2006): The Successive-Order-of-Interaction Radiative Transfer Model. Part I: Model Development. *J. Appl. Meteor. Climatol.*, 45, 1388–1402. DOI: http://dx.doi.org/10.1175/JAM2387.1.

[RD-08] Gómez-Chova, L., J. Muñoz-Marí, J. Amorós-López, E. Izquierdo-Verdiguier, and G. Camps-Valls (2013): Advances in synergy of AATSR-MERIS sensors for cloud detection, Geoscience and Remote Sensing Symposium (IGARSS), DOI: http://dx.doi.org/10.1109/IGARSS.2013.6723808.

2 The Microwave Radiometer series

2.1 Characteristics of the Microwave Radiometer

The Microwave Radiometers (MWR) flown on-board the ERS-1, ERS-2 and Envisat missions are two-channel nadir-pointing passive microwave instruments measuring top-of-the-atmosphere (TOA) brightness temperatures (see Table 1 for more details). A similar instrument will be flown on board the future Sentinel-3 missions.

Table 1: Main characteristics of the Microwave Radiometer series[1].

Absolute accuracy	Brightness temperature: ca. 2.6 K
3-dB beam width	1.5 degrees
Spatial resolution	20 km (from an altitude of approx. 780 km)
Swath width	20 km
Frequencies	23.8 GHz and 36.5 GHz
MWR lifetime (*)	ERS-1: 07/1991-06/1996 ERS-2: 04/1995-07/2011 Envisat: 03/2002-04/2012

(*): See also Table 2

2.2 Applications of Microwave Radiometer observations

The main purpose of the Microwave Radiometers is the measurement of the tropospheric path delay for the altimeter through the measurement of the atmospheric integrated water vapour content and the estimate of the attenuation of the altimeter signal by cloud liquid water content. This is achieved by measuring the brightness temperature (Tb) at 23.8 and 36.5 Ghz which are, over ocean, sensitive to the content of water vapour and liquid water in the troposphere, respectively. Combined with the altimeter backscattering coefficient (sigma0), the measured Tbs allow for a determination of the wet tropospheric correction (WTC) accounting for altimeter path delays caused by the water vapour content in the atmosphere. Due to its large amplitude as well as spatial and temporal variability, WTC is the most critical correction in the altimeter error budget.

Beyond their use in altimetry, the global time series on total column water vapour (TCWV) and cloud liquid water content retrieved by the MWR instruments have a high scientific value per se due to the paramount importance of clouds and water vapour in the climate system.

[1] Envisat/RA-2/MWR Product Handbook: http://earth.esa.int/pub/ESA_DOC/ENVISAT/RA2-MWR/ra2-mwr.ProductHandbook.2_2.pdf

2.3 Life cycles of Microwave Radiometers

Table 2 sums up the main events during the lifetimes of MWR on board ERS-1 and ERS-2.

Table 2: Life cycles of the MWR instruments on-board ERS-1, ERS-2 and Envisat.

Time	MWR on ERS-1	MWR on ERS-2	MWR on Envisat
1991/07/17	Launch		
1991/07/17 – 1991/12/28	35-day period		
1991/12/28 – 1992/03/30	3-day period		
1992/03/30 – 1993/12/24	35-day period		
1993/12/24 – 1994/04/10	3-day period		
1994/04/10 – 1995/03/21	168-day period		
1995/03/21 – 1995/05/15	35-day period		
1995/04/21		Launch	
1995/05/15 - 1996/06/02	ERS-1 and ERS-2 on identical orbits (35 days) with a 1-day shift		
1996/06/02	Switch off		
1996/06/26		Gain drop on 23.8 GHz. 23.8 Ghz starts drifting (1)	
2000/03/31	Retired		
2002/03/01			Launch
2003/06/22		Tape recorder incident (2)	
2011/07/06		Retired	
2012/04/08			Connection to Envisat lost

(1) After pass number 650 in cycle 12: gain drop in the 23.8 GHz channel probably due to an amplifier break down. From this date, a drift on 23.8 GHz TB is also detected.

(2) Tape recorder A stopped functioning. Only real-time observations could be supported after that date with the spacecraft returning data when in line of sight of an appropriately equipped ground station. Since the majority of such stations are found around Europe and Canada, good ERS-2 coverage of these regions including the North Atlantic could continuously be achieved.

2.4 Generation of the EMiR brightness temperature dataset

It was originally intended to use the REAPER v1.0 dataset[2] [3] of MWR brightness temperatures for the purposes of the EMiR project. However, the validation of the REAPER v1.0 dataset revealed some anomalies in the ERS-1 and ERS-2 MWR brightness temperatures and associated water vapour due to the intercalibration with Envisat MWR v2.0 brightness temperatures, which served as a reference. Indeed, as detailed in the related announcement on ESA web site[4], the Envisat MWR v2.0 Tb dataset suffers from in-flight calibration issues. It was therefore required to re-generate the entire MWR Tb time series to meet the requirements of fundamental and thematic climate data records. The newly derived EMiR Tb dataset benefits from the most up-to-date processing for each of the three missions and the best consistency over the whole time period covered.

2.4.1 Envisat MWR

The Envisat MWR dataset v2.1b used herein has been generated by CLS in 2014 in the frame of the Envisat MWR L1B Expert Support Laboratory (ESL) activities funded by ESA. It consists of a corrected dataset that removes the anomaly that has been observed in version 2.0. The brightness temperature time series presented below in Figure 1 for both channels were used to estimate the v2.1b wet tropospheric correction, which has been fully validated and shows the best performance [reference].

2.4.2 EMiR reprocessing of ERS-1 and ERS-2

The ERS-1 and ERS-2 MWR brightness temperatures have been entirely reprocessed in the frame of the EMiR project.

- The so-called "1st run" REAPER L1B dataset is the basis for this reprocessing. This "1st run" processing is an expert product, not distributed to users, and does not include any inter-calibration processing so it does not suffer from the known issues of the REAPER v1.0 Tb dataset. (Note that intercalibration activities are a key task within EMiR).
- The "1st run" REAPER L1B dataset already benefits from a strong consolidation of the L0 dataset with major gap filling and from the update of the side-lobe correction (the same as used to generate the Envisat v2.1b dataset).
- Since the "1st run" REAPER L1B is dated at the radiometer time tag, a linear interpolation is applied to collocate ERS-1 and ERS-2 MWR Tbs on the altimeter time tag.
- Land measurements are discarded and no specific processing is applied in coastal areas so that contamination from land may occur above coastal waters at distances of less than ca. 50km from land.

---

[2] ESA announcement on REAPER availability: https://earth.esa.int/web/guest/missions/esa-operational-eo-missions/ers/news/-/article/reprocessed-esa-ers-altimetry-reaper-dataset-now-available

[3] REAPER Product Handbook: https://earth.esa.int/documents/10174/1511090/Reaper-Product-Handbook-3.1.pdf

[4] https://earth.esa.int/web/guest/missions/esa-operational-eo-missions/envisat/news/-/article/envisat-ra2-updated-mwr-wet-tropospheric-correction-for-altimetry-v2-1-dataset

- No additional processing is applied to ERS-1 (both MWR channels) and the ERS-2 MWR 36.5 GHz channel. However, a correction of the gain drop and the drift on the ERS-2 MWR 23.8 GHz channel is applied, following the recommendations proposed in [RD-02]:
  - The following linear correction accounts for the gain drop that occurred in June 1996:

```
TB23.8corrected_for_the_gain_drop = 0.93 x TB23.8 + 19.18
```
(1)

  - Since the gain drop, a drift appeared as well on the 23.8 GHz brightness temperatures [RD-02]. An additional correction term was then proposed to account for this effect:

```
TB23.8corrected_for_the_gain_drop_and_from_the_TBs_drift =
TB23.8corrected_for_the_gain_drop +
corr(t,TB23.8corrected_for_the_gain_drop)
```
(2)

with:

```
corr(t, TB23.8corrected_for_the_gain_drop) = 0 for t ≤ 1.18
corr(t, TB23.8corrected_for_the_gain_drop)= (a1*t+a2)*
TB23.8corrected_for_the_gain_drop + (b1*t+b2) for t > 1.18
  • a1=-0.001521
  • b1=0.4564
  • a2=0.001795
  • b2=-0.5386
```
(3)

where *t* is the elapsed time in decimal years since the launch of ERS-2.

Table 3 sums up the processing applied to ERS-1 and ERS-2 data in order to derive the EMiR Tb data set.

Table 3: Processing of ERS-1 and ERS-2 MWR brightness temperatures for generation of EMiR L1B dataset.

ERS-1 and ERS-2 Tb dataset processing for EMIR	
L1B source	Basis is the REAPER “1st run” (non-public) dataset: ➢ L0 consolidation (e.g. gap filling) ➢ Envisat side-lobe correction algorithm applied
Interpolation on altimeter time tag	Linear interpolation is applied to collocate MWR with the altimeter time tag
Surface coverage	Surface coverage is limited to ocean and sea ice, land surfaces are discarded
Coastal corrections	No specific coastal processing is applied, land contamination is possible for distances to coast <= 50 km
ERS-2 23.8 GHz channel	Corrections have been applied to correct gain drop and drift observed in the ERS-2 MWR 23.8 GHz channel after 1996-06-26

Figure 1 shows a daily-mean time series of the EMiR Tb dataset, focussing on the ERS-1 and ERS-2 time series (only the first year of Envisat observations is shown here). The applied correction significantly reduces the drop and drift effects in the ERS-2 channel at 23.8 GHz (light blue: original data, dark blue: corrections applied), but a transition period is still observed before the stabilization of the Tb.

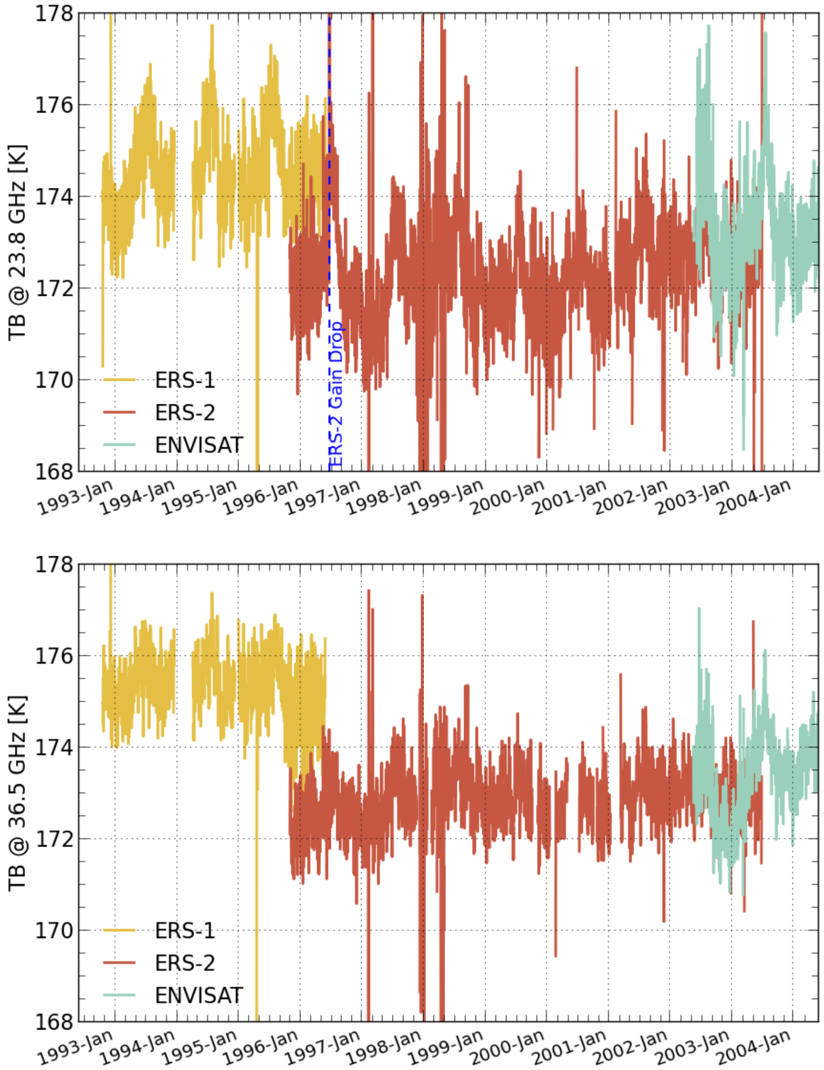

Figure 1: MWR Tb datasets (valid ocean) provided to the EMiR consortium. Top: 23.8 GHz channel for ERS-1 (gold), ERS-2 (red), and Envisat (turquoise). Bottom: As above, but for the 36.5 GHz channel.

3 Calibration assessment strategy

Within the framework of EMiR, the aforementioned MWR dataset has undergone an independent and detailed calibration assessment. The goal was to independently assess the accuracy and stability of the dataset provided and to lay the ground for subsequent intercalibration activities with the ultimate goal of creating an FDR.

In order to establish a baseline for the calibration assessment, two different radiative transfer models were used to calculate biases between simulated and observed brightness temperatures. Note that because of the difficult absolute calibration of microwave instruments and various uncertainties in the forward models, it is not expected that models and observations match perfectly. For a discussion of issues related to bias assessments, see also [RD-05]. The two models used are:

- RTTOV [RD-06] which will be the model used in the operational water vapour retrievals envisioned within EMiR.
- In addition, another model, SOI [RD-07], combined with FASTEM-5 [RD-05] was used to also calculate brightness temperatures and to provide an assessment independent of RTTOV.

Comparisons were performed using ECMWF ERA-Interim reanalysis of surface wind speed, sea surface temperature, and profiles of temperature, cloud liquid water, and water vapour. See [RD-03] for more information on the radiative transfer models and the particular setup of the simulations used here.

In addition to the bias assessment, a set of sensitivity studies were carried out in order to further assess particular contributions of different error sources. In particular:

- A sensitivity run was performed using the CLS-derived water vapour and cloud liquid water values to rescale the ECMWF profiles water vapour and liquid water profiles. This test allows for a partial assessment of the consistency between the CLS-derived water vapour retrievals and the models used herein.
- Another sensitivity run was performed using known cloud-free observations (from collocated FAME-C MODIS/AATSR cloud fraction (see Section 4.2) with simulated cloud-free brightness temperatures. This comparison strategy eliminates cloud liquid water as a source of uncertainty and allows for a better understanding of causes for remaining biases.

In order to avoid possible contamination of observed brightness temperatures with land or sea ice, only areas at a distance of more than 100 km from land or sea ice were considered. The processes and datasets used for land- and sea ice flagging are described in the MWR Level 2 ATBD [RD-03].

Data were evaluated for the latitude bands ±30 degrees, ±60 degrees, and globally. Time series of biases (observations minus simulations) have been produced as well as tables summarizing the results and are presented in Section 4.

4 Results

4.1 MWR data availability

Figure 2 and Figure 3 provide an overview on the availability of MWR data. On average, a little more than one million (average: 1,046,370) observations per month fit the data selection criteria laid out in Section 3. These numbers do not differ very strongly between the three satellites. Restricting the dataset to the latitude range between 60 degrees N/S reduces the number of available monthly observations to slightly less than one million (average: 968,597). Restricting the latitude range further to 30 degrees N/S reduces this number further to 483,425 or slightly less than fifty percent of the total dataset.

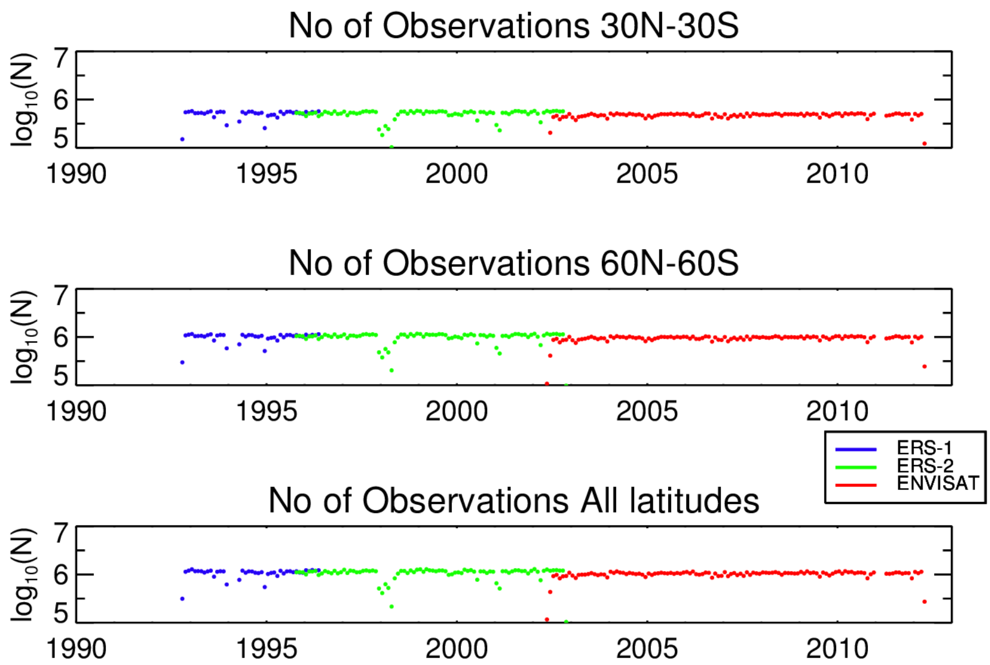

Figure 2: Monthly data availability for the entire observation period and for the three latitude bands 30 N – 30 S (upper panel), 60 N – 60 S (middle panel) and for all latitudes (lower panel). All numbers are in observations per month.

One can also deduce from Figure 2 that the coverage over the entire lifetime of the satellites is fairly homogeneous with a few exceptions mostly near the beginning and end of the lifetime of the satellites.

Figure 3 shows the spatial distribution of observations for the three satellites. Note, data closer than 100 km from either coast or sea ice have been excluded from the comparison as per the criteria outlined in [RD-03]. Hence, the data density close to coasts or sea ice is near zero. Above the open ocean, each 1×1 degree grid box typically contains about 30 observations per month.

Note that the grid pattern apparent over the oceans for most of the latitudes is caused by the orbit progression of the three satellites. Thus, for example in the central Pacific a certain grid box contains on average 45 observations per months, whereas an adjacent grid box only contains 24 observations per month. This pattern starts to vanish for larger grid boxes and almost completely smoothes out for 3×3 degrees average (see Figure 4). Thus, for any final gridded product, a target resolution no higher than 2×2 degrees appears advisable.

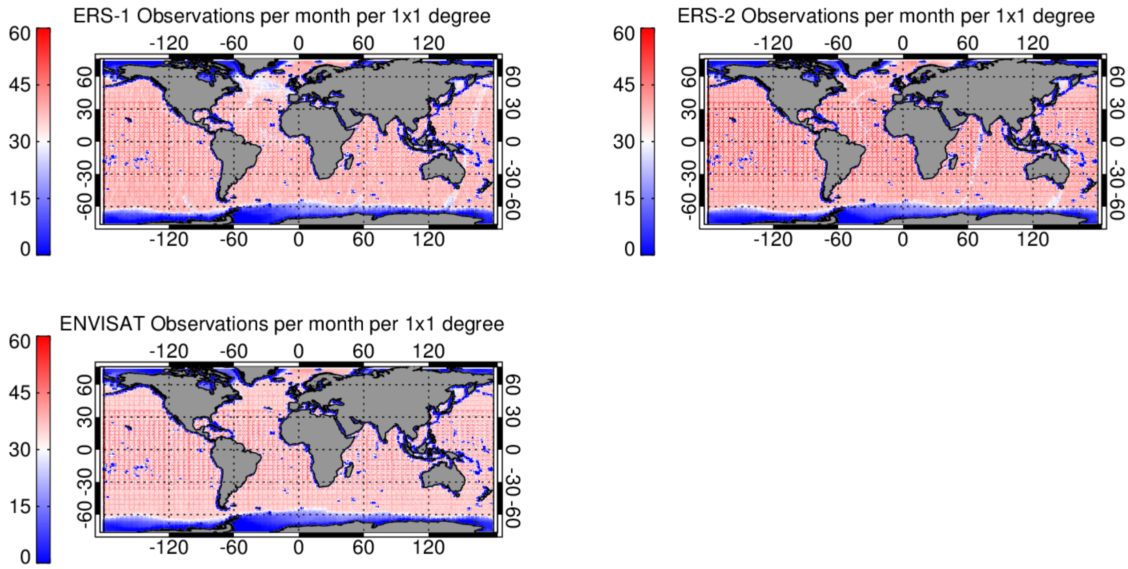

Figure 3: Average MWR data availability per month and 1×1 degree grid box.

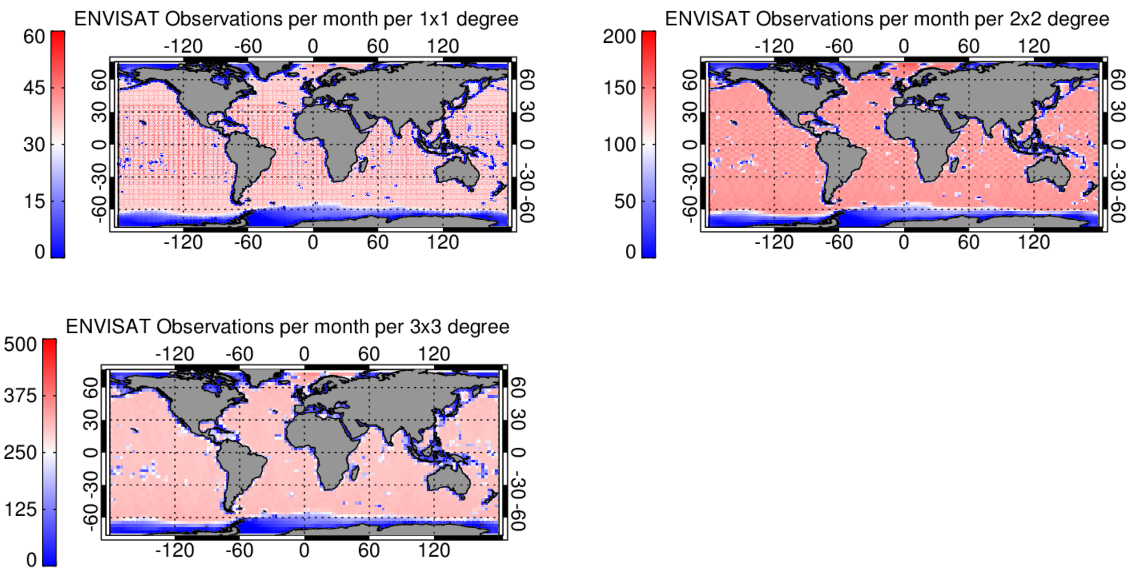

Figure 4: Average data availability per month for MWR on Envisat as function of the size of the averaging grid box (1×1 degree top left panel, 2×2 degree top right panel, and 3×3 degree bottom left panel).

4.2 Cloud screening

The Freie Universität Berlin AATSR MERIS Cloud (FAME-C) cloud mask [RD-04] has been used to identify and subsequently exclude cloud affected observations from further analyses to test the impact of clouds on the MWR bias assessment. Since this cloud mask relies on MERIS and AATSR this investigation can only be performed for Envisat MWR observations.

The FAME-C cloud mask is based on a Bayesian approach. The probability for cloud occurrence under the condition of having a feature **F** is calculated by:

$$P(C_{yes}|\boldsymbol{F}) = \frac{P(C_{yes})P(\boldsymbol{F}|C_{yes})}{\mathrm{P}(\boldsymbol{F})}, \qquad (4)$$

where $P(C_{yes})$ is the probability of cloud occurrence, $P(\boldsymbol{F}|C_{yes})$ is the probability of occurrence of the feature **F** under the condition of having a cloud, and $\mathrm{P}(\boldsymbol{F})$ is the probability of having feature **F**. **F** can be a vector of any dimension, e.g. a measurement spectrum. All variables on the right hand side can be approximated through a probabilistic approach and appropriate reference data, in this case the AATSR/MERIS synergy cloud mask described in [RD-08]. The operational version of FAME-C employed here mainly uses the following four channel combinations as features: M900*M753, A12.0*A3.7, M510/A3.7, M865/M885, where M refers to MERIS and A to AATSR channels, respectively. In case of channel saturation or missing data, other channel combinations have been applied. Further information on feature selection can be found in [RD-04].

FAME-C provides cloud probabilities between 0 and 100 Percent. Global data are available for the years 2007, 2008, 2009. The collocation scheme was performed as follows: All available FAME-C data were spatially and temporally collocated with the corresponding MWR path. Only data over the ocean were used (Figure 5). Cloud probabilities were then assigned to each MWR pixel. To be able to account for the footprint of the MWR measurements of about 20 km in diameter, the side lobes, and potential navigational inaccuracies, the cloud probability was averaged over four different areas around the centre of MWR footprints: 25×25 km^2, 50×50 km^2, 100×100 km^2, and 200×200 km^2 (Figure 6). In order to make the data more convenient to use, the fraction of pixels that were below a certain cloud probability threshold value was stored for each area. This was done for the following cloud probability bins: 0%, 1%, 2%, 5%, 10%, 20%, 30%, 40%, 50%, 60%, 70%, 80%, 90%, 100%. This yields to a data set that contains the geolocation of the MWR track, the bin information and the fraction of cloud probabilities for each MWR data point.

For the purpose of this study, MWR observations were deemed cloud-free if the FAME-C derived cloud likelihood did not exceed 10% within a 100 x 100 km neighbourhood around the centre of the MWR footprint.

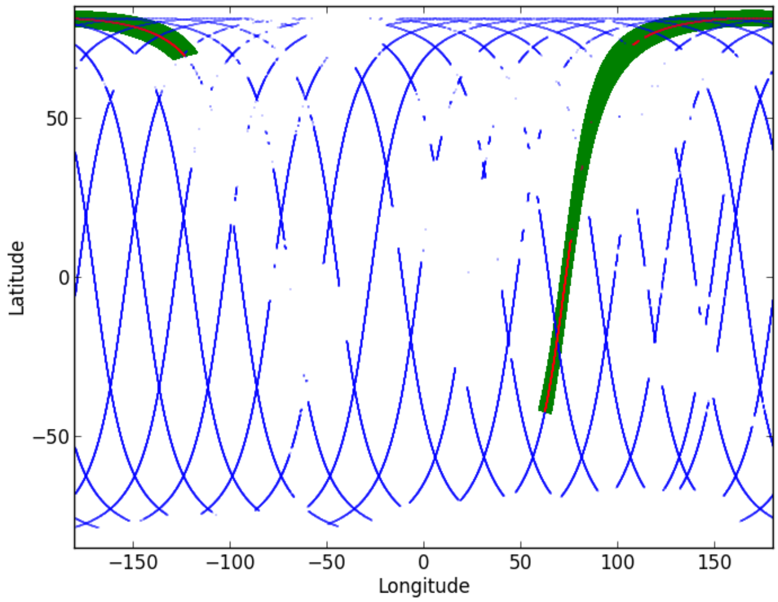

Figure 5: Example of the collocation of the MWR track (blue, only available above the ocean) with the MERIS/AATSR FAME-C cloud mask (green, with matching MWR data in red for better contrast) for parts of an orbit.

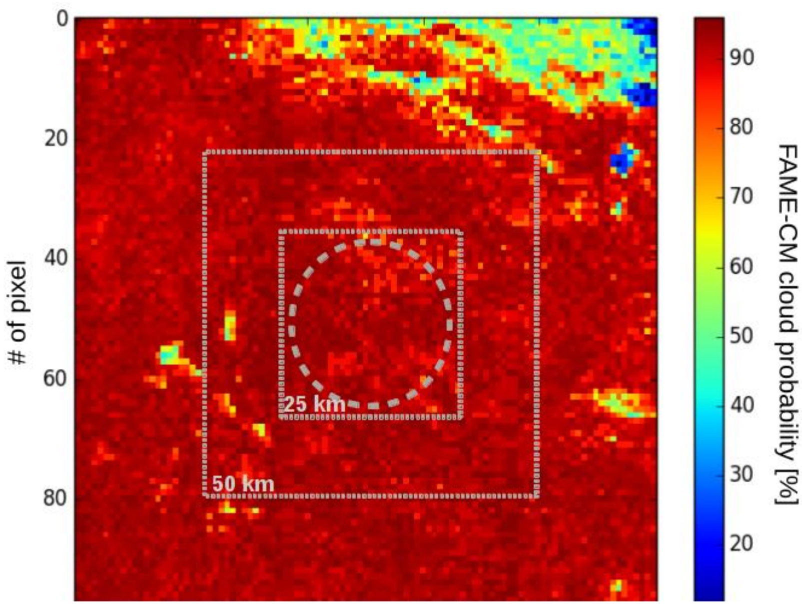

Figure 6: Example of a 100×100 km² segment of the FAME-CM cloud probability field. The circle displays the approximate MWR footprint. The inner squares indicate averaging areas of 25×25 km² and 50×50 km².

4.3 ERA-Interim profiles

Each MWR data point was collocated with the spatially closest ERA-Interim temperature and water vapour profile. In addition, a set of important surface parameters was also collocated. The ERA-Interim data were converted to the 43 RTTOV standard pressure levels. In the process of remapping to RTTOV pressure levels, it was ensured that total column water vapour (TCWV) and liquid water path (LWP) were conserved. All data for one day were collocated to the ERA-Interim analysis valid for 12:00 UTC on that day. Table 4 lists the available parameters.

Table 4: Available ECMWF ERA-Interim parameters mapped onto MWR pixels.

Name	Parameter	Unit	Type
SST	Sea surface temperature	K	Surface
WIND	Wind speed at 10 m above sea surface	m/s	Surface
TCWV	Total column water vapour	kg/m^2	Surface
LWP	Liquid water path	kg/m^2	Surface
P	Pressure on RTTOV levels	Pa	Profile
T	Temperature on RTTOV levels	K	Profile
Q	Water vapour mixing ratio on RTTOV levels	g/kg	Profile
L	Liquid water mixing ratio on RTTOV levels	g/kg	Profile
Z	Height above surface on RTTOV levels	m	Profile

4.4 Brightness temperature biases and standard deviations

4.4.1 Global analysis

Table 5, Figure 7, and Figure 8 (Figures shown in Annex) present the overall bias and standard deviation (observations minus simulations) statistics for the three MWR instruments for 23 and 36 GHz. The comparisons follow the strategy outlined above in Section 3 and exclude any observations closer than 100 km to sea ice or land surfaces.

Biases for 23 GHz are consistent over time with only a very weak annual cycle (< 1 K). ERS-2 exhibits a somewhat larger bias than the two other instruments, which are generally in good agreement with each other. At 36 GHz, Envisat shows a somewhat larger annual cycle than the other two instruments and ERS-1 again shows enhanced bias values.

Table 5 also shows global mean comparisons between the two different radiative transfer models used in this study. In all instances RTTOV shows smaller biases than SOI/FASTEM, indicating a better agreement between REAPER and RTTOV and justifying the choice of RTTOV as the standard radiative transfer model to be used in the retrievals.

Table 5: Global bias and standard deviation (STDV) statistics (observations minus simulations) for all MWR instruments. The first number gives the bias against RTTOV. The second number (in brackets) gives the bias against an independent radiative transfer model (SOI/FASTEM).

	23 GHz Bias [K]	36 GHz Bias [K]	23 GHz STDV [K]	36 GHz STDV [K]
Envisat	3.3 (6.2)	6.2 (9.4)	9.4 (8.6)	10.3 (10.2)
ERS-1	5.1 (8.1)	8.4 (11.6)	9.5 (8.8)	10.8 (10.7)
ERS-2	2.7 (5.7)	5.8 (9.0)	9.4 (8.7)	10.8 (10.7)

Standard deviations between observations and simulations are given in Figure 9 and Figure 10 (figures in annex). Standard deviations are in the order of 10 K independent of satellite instrument and radiative transfer model used. These standard deviations are reflecting mostly uncertainties in the description of the state of the atmosphere by ERA-Interim and are expected. In fact, the task of any subsequent retrieval is to improve over the first-guess state of the atmosphere provided by ERA-Interim and find values of total column water vapour and liquid water path that minimize the remaining discrepancies in brightness temperature space.

4.4.2 Regional effects

Figure 11 and Figure 12 (figures in annex) show the spatial distribution of biases for all three instruments and for both channels. It is interesting to see that especially at 23 GHz major outflow areas west and south of the continents show high biases, in particular off the coast of north-western Australia, the Arabian Sea, and off the west coast of northern Africa. These biases are likely not artefacts but occur in regions where ERA-Interim predicts either too few clouds or too dry an atmosphere. Other areas including the Red Sea, the Mediterranean, and some spots at high latitudes are likely still affected by land and/or sea ice contamination. For example, the Red Sea is around 270 km wide at its widest point. Because of the required minimum distance from coast of 100 km only few data points are kept for analysis. However, these data points might still be partially contaminated by land via side lobe effects or navigation uncertainties. At 36 GHz biases show similar patterns but are generally enhanced in areas with higher cloudiness, such as the Intertropical Convergence Zone. These effects are expected because the first guess cloud profile from ERA-Interim is not expected to represent the actual cloud conditions very, in particular in situations with convective clouds.

4.4.3 Identifying error sources

In order to separate instrument-related and forward model-related biases from any biases introduced by the first guess, two more experiments were performed. In a first experiment, the water vapour and liquid water in the first guess were scaled to agree with the CLS retrievals. In a second experiment, cloud liquid water was set to zero and only cloud-free observations were compared. The results of these two experiments are summarized in Figure 13 to Figure 16 (figures in annex) as well as Table 6 and Table 7 below.

The results of these scaling experiments suggest that large parts of the biases discussed above are indeed associated with the representativeness of clouds in ERA. For example, under cloud-free conditions (determined using the FAME-C cloud mask), the standard deviation of the 36 GHz channel is reduced from 10 K to only about 2 K (compare and Table 7). Similar reductions are observed in biases especially at 23 GHz.

Table 6: Global bias and standard deviation statistics (observations-simulations) after rescaling with CLS-derived water vapour and liquid water path (Envisat only). Radiative transfer model SOI/FASTEM.

	23 GHz Bias [K]	36 GHz Bias [K]	23 GHz STDV [K]	36 GHz STDV [K]
Envisat	**5.2**	**6.6**	**3.2**	**2.0**

Table 7: Global bias and standard deviation statistics (observations-simulations) for cloud-free cases identified through the collocated FAME-C cloud mask (Envisat only, 2007-2011). Radiative transfer model SOI/FASTEM.

	23 GHz Bias [K]	36 GHz Bias [K]	23 GHz STDV [K]	36 GHz STDV [K]
Envisat	2.8	6.7	4.4	2.4

4.4.4 Summary on error sources

In summary, the reported biases and standard deviations include contributions from the following error sources:

1. Representativeness of ERA-Interim analysis for the actual observation (e.g. wind gusts modifying surface emissivity, representation of clouds),
2. Spatial and temporal colocation errors between ERA-Interim analyses and MWR observations,
3. Calibration biases/errors of the different MWRs,
4. Systematic errors and uncertainties in the surface emissivity model,
5. Systematic errors and uncertainties in spectroscopy of liquid water absorption, dry air absorption, and water vapour absorption,
6. Impact of precipitation contamination and precipitation-ice scattering not accounted for in the forward model.

While the first two items on this list have a significant impact on the values reported here, they only play a secondary role for the retrieval accuracy. In fact, the main task of the retrieval will be to find an optimal solution of the atmospheric state that is consistent with the observations, thereby minimizing the initial deviation between first guess and observations.

The latter four items in the above list, while having smaller contributions to the overall bias, are of crucial importance to the accuracy and long-term stability of an FDR. These will need to be addressed in an empirical bias-correction scheme as outlined below.

5 Conclusions

The assessment of the MWR calibration leads to the following conclusions:

- The calibration of MWR is stable and ERS-2 and Envisat appear to be well inter-calibrated. Globally and annually averaged biases of ERS-2 and Envisat observations as compared to simulations are around +3 K for 23.8 GHz and +6.0 K for 36.5 GHz using RTTOV.
- Similar, but slightly increased biases are found using another radiative transfer model (SOI/FASTEM) with globally and annually averaged biases of ERS-2 and Envisat observations as compared to simulations of around +5 K for 23.8 GHz and +10.0 K for 36.5 GHz.
- ERS-1 is further biased by an additional about +2 K against ERS-2 and Envisat in both channels. Results obtained as part of this study are in general agreement also with the independent assessment performed by CLS (Envisat only).
- Causes for those biases include the difficult absolute calibration of the MWRs as well as uncertainties in the surface emissivity and spectroscopic models used.
- The variability of these biases is low so that effective bias-cloud correction and inter-calibration schemes can be devised.
- In addition to the global results, the impact of clouds was also studied using the FAME-C Bayesian cloud mask based on MERIS and AATSR observations. The combination of this product with MWR on Envisat was straightforward and allows to easily identify cloud-free regions for assessing water vapour spectroscopy and surface emissivity. Combination of similar products (MWR plus SLSTR, OLCI) for Sentinel-3 is regarded as highly beneficial.

6 Recommendations and Outlook

Based on the findings presented herein, the following course of action for the current project is recommended:

- The current implementation of RTTOV (outcome of the ESA DUE GlobVapour activities) provides excellent comparisons with the MWR brightness temperature time series and shall be used in the framework of the optimal estimation retrieval for water vapour and liquid water processing.
- Using this set of models, the following issues will need to be tackled:
    - A bias correction/intercalibration scheme will need to be devised. This will require some additional calculations using RTTOV, including the calculation of cloud-free brightness temperatures.
    - Derivation of initial TCWV and LWP time series. This will include a first bias-corrected time series of water vapour.
    - Screening of strongly precipitating areas. A proposed approach is to evaluate brightness temperature residuals, the cost functions, and a posteriori errors. Collocated MERIS/AATSR data could be applied to help verifying screening approaches for Envisat.
    - Validation of initial time series.
- As for a surface emissivity model, it is recommended to currently continue using FASTEM.
- On a longer term, it would be desirable to develop a surface emissivity model that also includes the radar altimeter backscatter, so that one can use sigma_0 and possibly the significant wave height (SWH) to further constrain surface emissivity also for the radiometer frequencies. This is deemed highly beneficial but will likely not be possible within the current project.

7 Annex

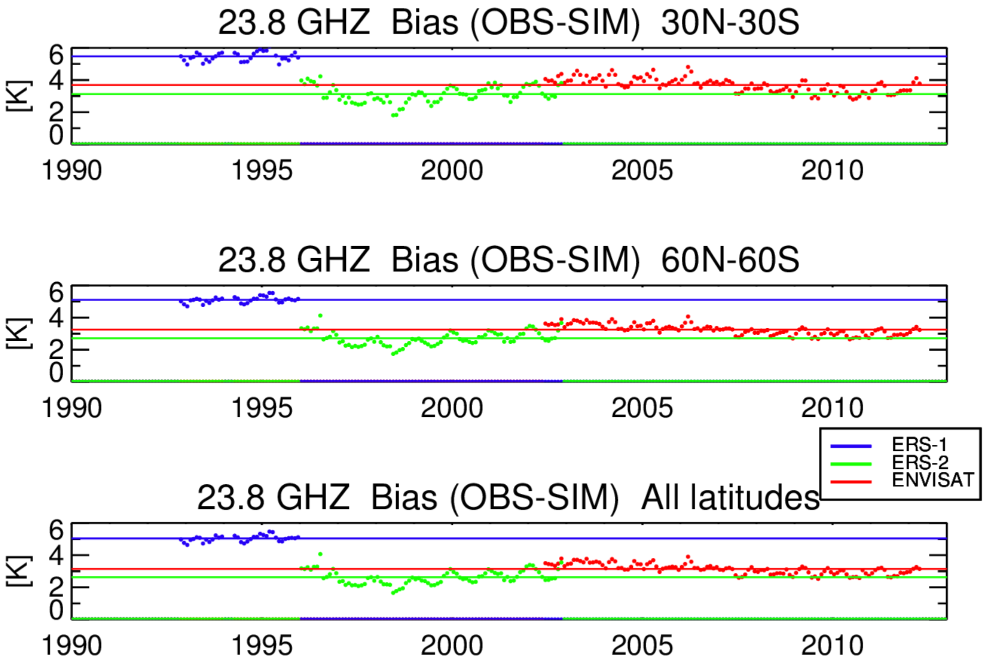

Figure 7: Time series of 23.8 GHz bias (observation minus simulation) for all three MWR instruments for the latitude bands described in Figure 2. Radiative transfer model: RTTOV.

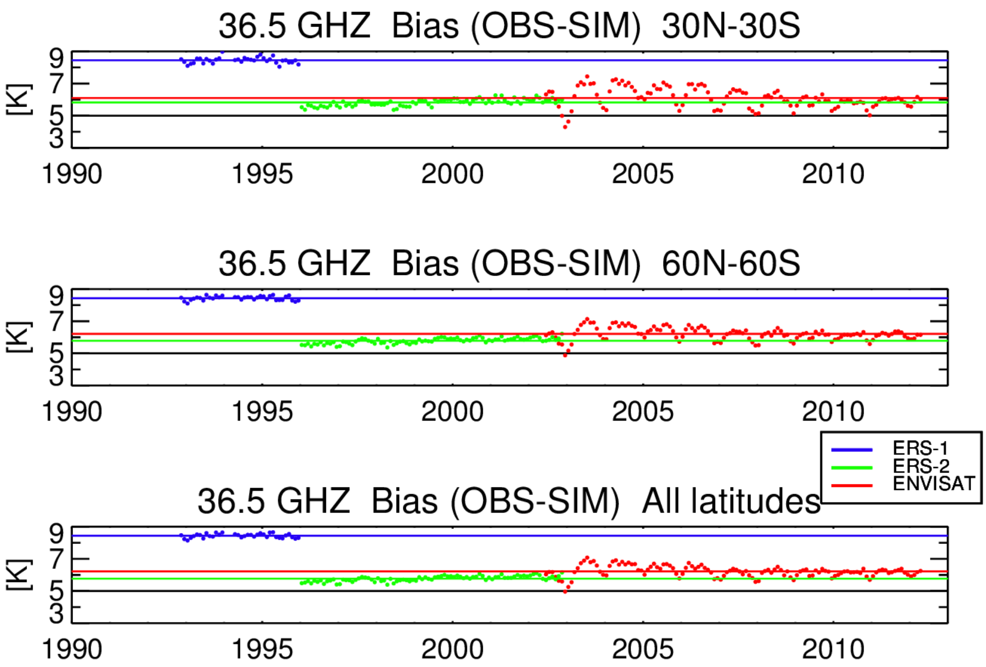

Figure 8: Same as Figure 7 but for 36.5 GHz. Radiative transfer model: RTTOV.

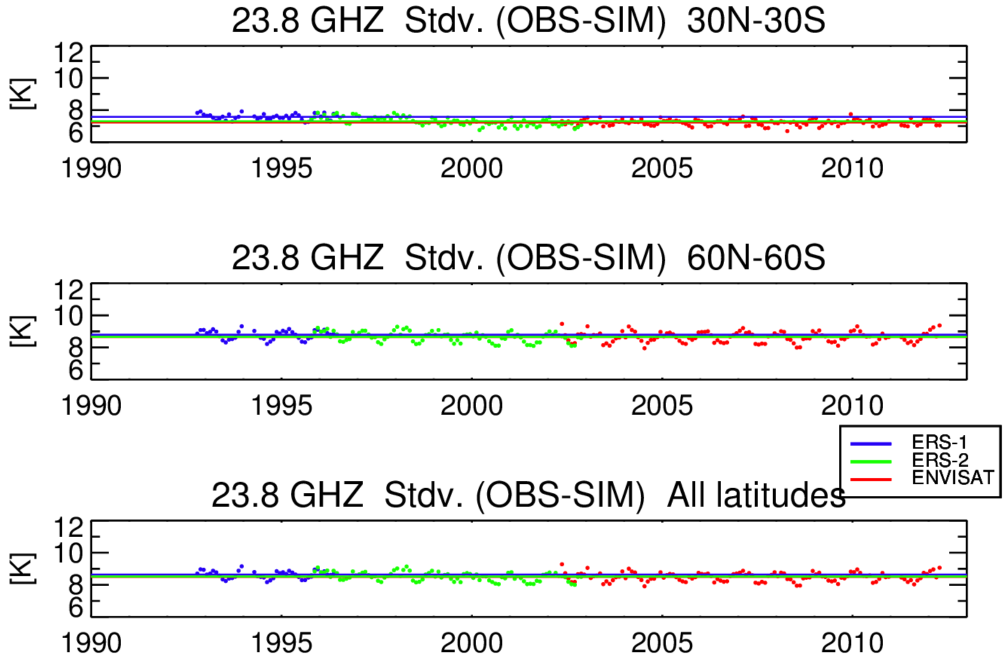

Figure 9: Standard dev. between 23.8 GHz observations and simulations for all three MWR instruments for the latitude bands described in Figure 2. Radiative transfer model: RTTOV.

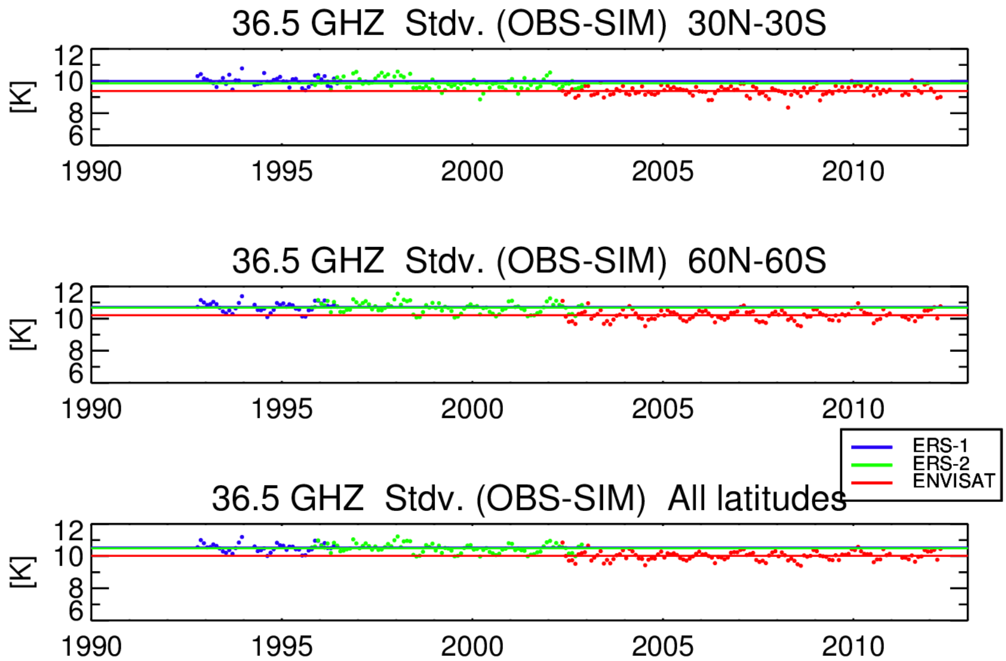

Figure 10: Same as Figure 9 but for 36.5 GHz. Radiative transfer model: RTTOV.

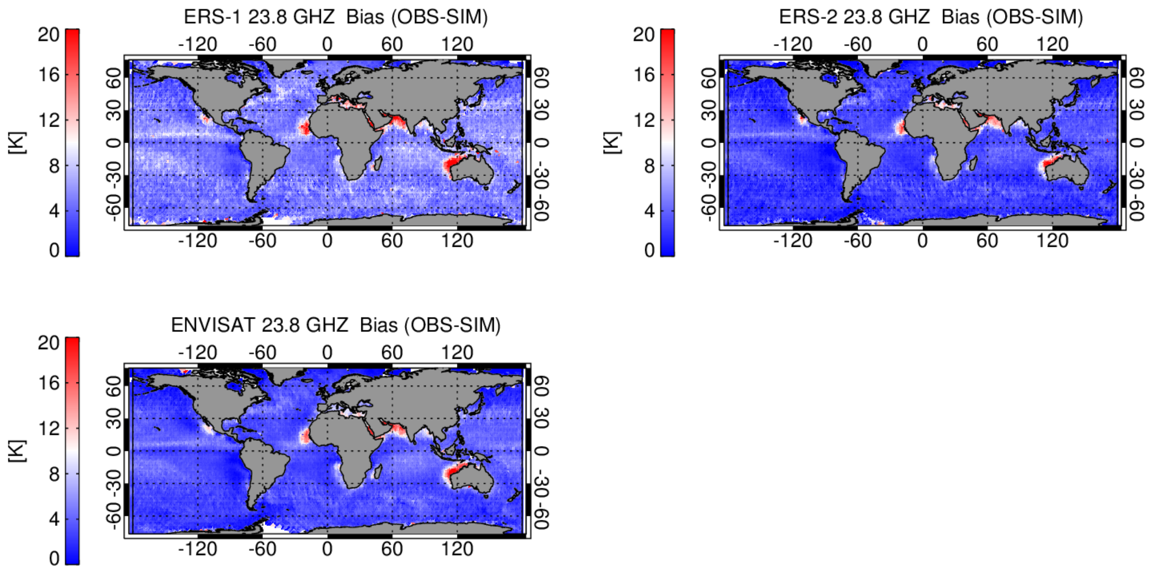

Figure 11: Spatial distribution of 23.8 GHz bias (observations minus simulations) for all three instruments averaged over their respective lifetimes. Radiative transfer model: RTTOV.

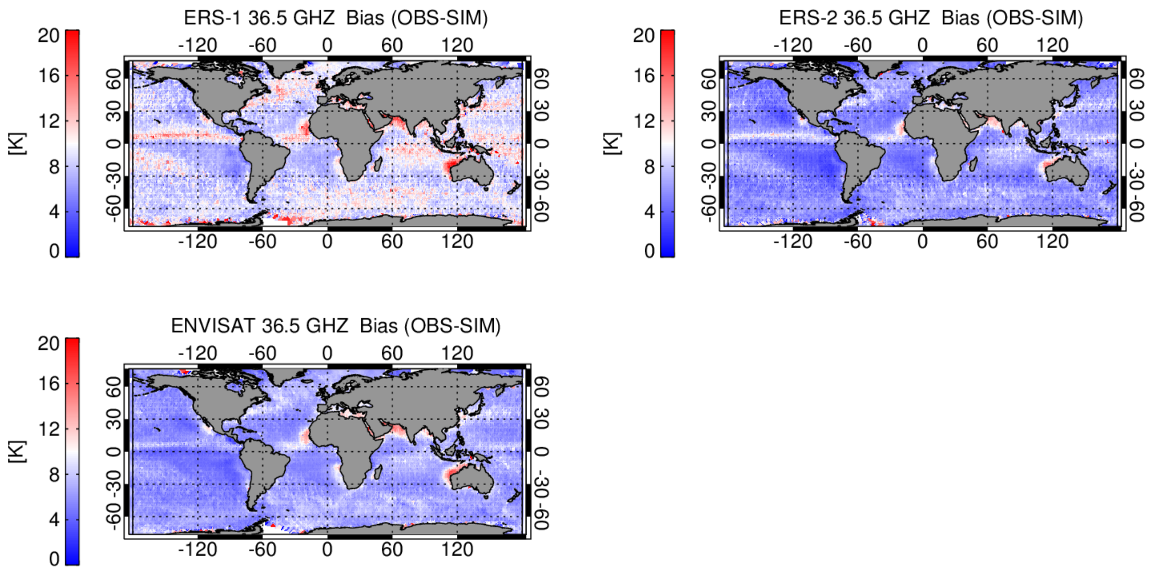

Figure 12: Same as Figure 11 but for 36 GHz. Radiative transfer model: RTTOV.

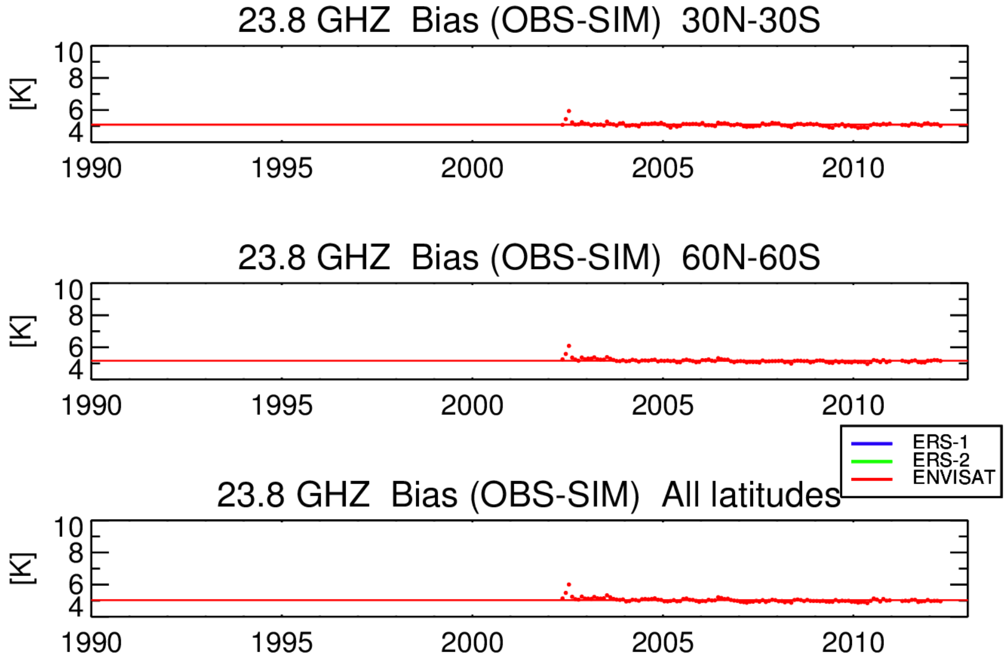

Figure 13: Same as Figure 7 but for scaled water vapour and liquid water path (Envisat only). Radiative transfer model: SOI/FASTEM.

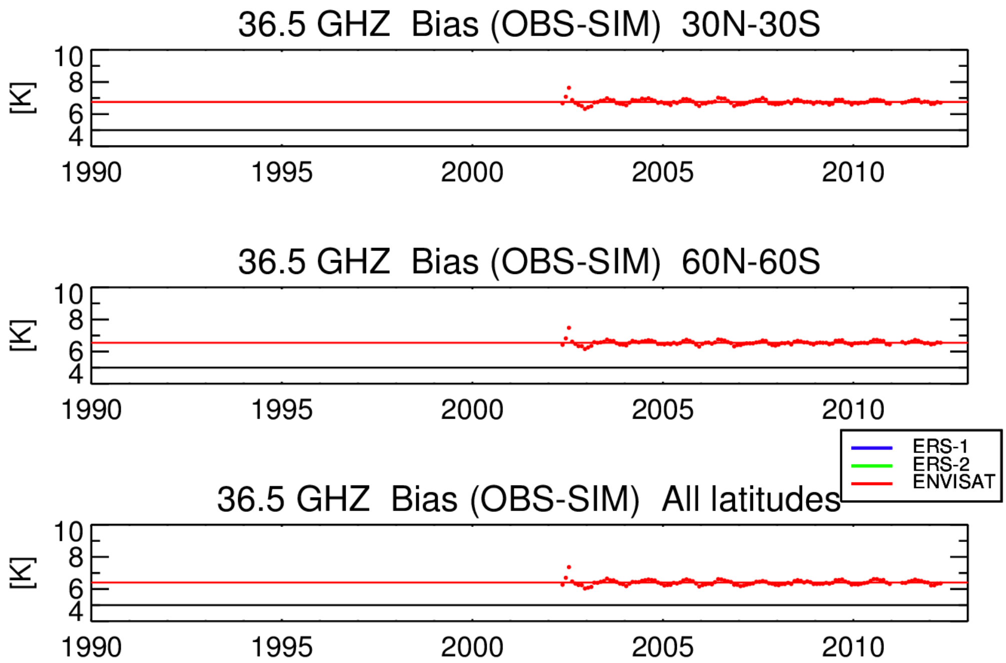

Figure 14: Same as Figure 13 but for 36 GHz. Radiative transfer model: SOI/FASTEM.

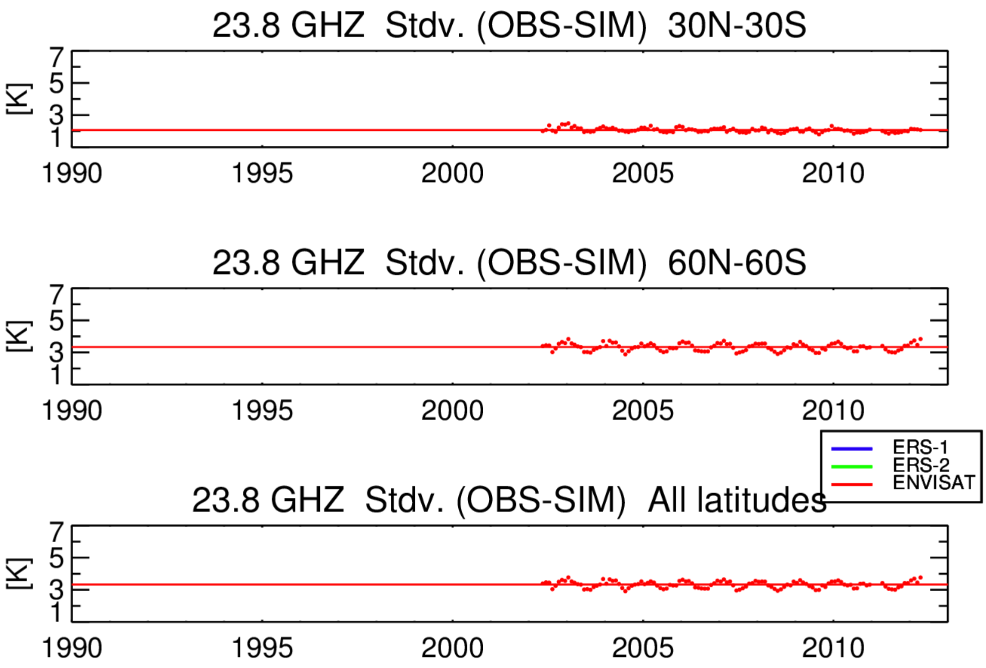

Figure 15: Same as Figure 9 but for scaled water vapour and liquid water path (Envisat only). Radiative transfer model: SOI/FASTEM.

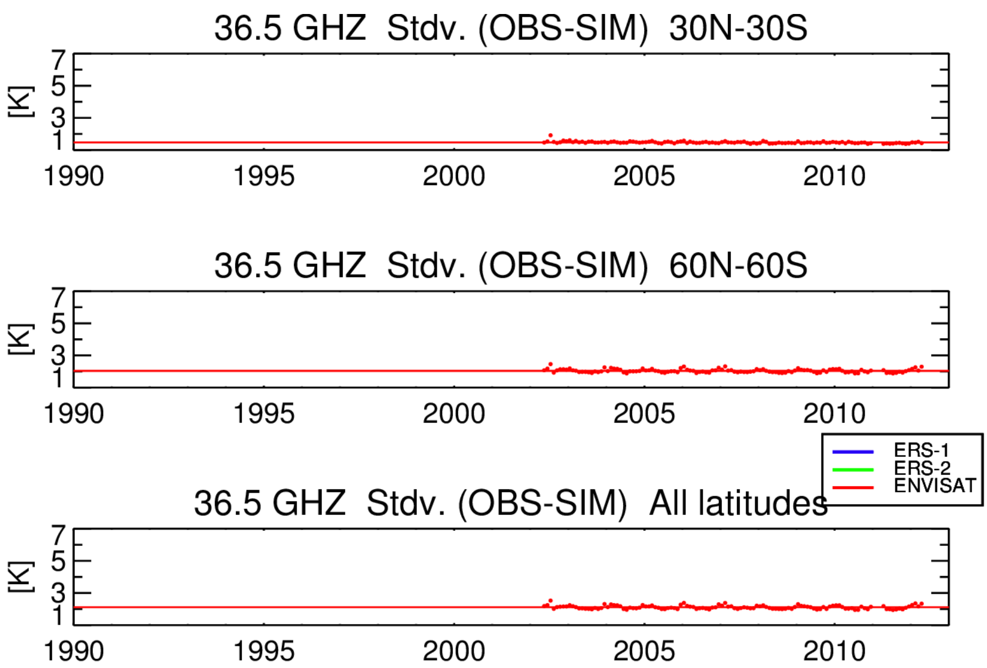

Figure 16: Same as Figure 15 but for 36 GHz. Radiative transfer model: SOI/FASTEM.